2024 IEEE International Conference on Robotics and Automation (ICRA 2024)
May 13-17, 2024. Yokohama, Japan

Design And Validation of a Variable Stiffness Spiral Cam Actuator (VS-SCA)

Matthew R. Auer, Suhrud P. Joglekar, and Hyunglae Lee*, *Member, IEEE*

Abstract— **This study presents the design and validation of a variable stiffness actuator incorporating multiple cam mechanisms. The actuator is intended for use in walking assistance, focusing on assisting individuals with diminished ankle function. This study highlights the advantages of variable stiffness actuators over traditional and other modern actuators in mobility assistance. The working principles of the proposed Variable Stiffness Spiral Cam Actuator (VS-SCA) are described, focusing on the cantilever beams with adjustable supports, main cam mechanism, and symmetric support positioning architecture utilizing an Archimedean spiral cam. The design and fabrication process are discussed, considering system design considerations, cantilever beam design, cam design, and spiral cam design. The analytical methodology used for validation is also presented, which connects the subsystems of the actuator and allows for the determination of effective torsional stiffness. The experimental validation showed that the VS-SCA provides a range of stiffness from 20 to 75 Nm/rad for dorsiflexion, necessary for providing ankle assistance during the push-off phase of walking, while maintaining low stiffness (4 - 12 Nm/rad) for plantarflexion not to hinder natural ankle motion in the swing phase.**

I. Introduction

Robotics is commonly used in mobility assistance where the robot is responsible for augmenting the individual user's abilities in the case of prosthetic devices, powered exoskeletons, or other wearable devices [1]. There are many approaches to mobility assistance, however the family of variable stiffness actuators has favorable properties for such applications.

Variable Stiffness Actuators (VSAs) are mechanisms designed with integral elasticity elements that allow for adjustment of the stiffness [2] based on the specific task or environment [3]. They pose significant benefits in the field of robotics for mobility assistance because VSAs can adjust their response to their environment, which can improve safety [4] and efficiency [5], especially in wearable devices where energy storage and release is utilized.

In comparison to traditional actuators such as direct drive, planetary gearbox, and cycloidal actuators, VSAs offer significant advantages for systems with high impulse and cyclic loads, particularly in mobility assistance applications, where lower extremity wearable assistive devices require substantial joint powers and velocities that would necessitate impractically large and heavy motors and gear ratio transmissions with traditional actuators. While modern actuators such as series elastic and parallel elastic actuators incorporate elastic elements in the gear train for force control and safety enhancement [2] and [6], they do not fully address the specific high impulse and cyclic load cases in which VSAs excel.

Various studies have explored VSAs development, focusing on design constraints and applications. There are two main types of VSAs: antagonistic motor setups involving co-contraction of elastic elements [7], [8], and independent motor setups [9] adjusting orthogonal spring properties for energy efficiency [10], [11]. Most of these designs have an increased part count, which introduces complexities, potential hysteresis loss [12] arises from the implemented mechanisms and elasticity of the part results in intricate controllers.

K. Guo et al. have created a radially symmetric VSA which uses S-shaped springs elements in turn adjusting the effective length of curved cantilever beams [13]. This device has a very large stiffness range but has very limited angular deformation in the range. The use of cam allows flexibility in non-linear torsional stiffness [14], [15], [16], [17]. Some designs use linkages and stacked cantilever beams to vary stiffness such as in the case of Choi et al [18]. However, these designs have high hysteresis due to frictional losses between the beams. While other mechanisms utilize lead screws for stiffness adjustment [18], [19], they tend to create oversized and heavy systems. Whereas Sun and Z. Guo's Archimedean spiral based VSA [20] achieves variable stiffness but results in a relatively thick actuator due to the multiple layers needed to attain a similar range of stiffness variation.

The objective of this study is to design and validate a VSA using multiple cams for various mechanisms to vary stiffness. The actuator will be designed around the case study of normal walking assistance, particularly in the later stance phase. The scope of this work is in the mechanical design and experimental validation of stiffness performance while future work will be in the usage of the device for walking assistance.

II. Working Principles

The Variable Stiffness Spiral Cam Actuator (VS-SCA) functions based on three principles: cantilever beams with adjustable supports, cams as means to convert linear stiffness to rotational stiffness, and symmetric Archimedean spiral cam for cantilever support adjustment (Fig. 1).

A. Cantilever Beams with Adjustable Supports

The Euler-Bernoulli beam theory [21] describes the deflection of the neutral axis due to applied loads and given

* Corresponding author (email: hyunglae.lee@asu.edu)

This work was funded by the National Institute of Arthritis and Musculoskeletal and Skin Diseases of NIH under Award Number R01AR080826. The authors are with the School for Engineering of Matter, Transport and Energy, Arizona State University, Tempe, AZ 85287, USA.

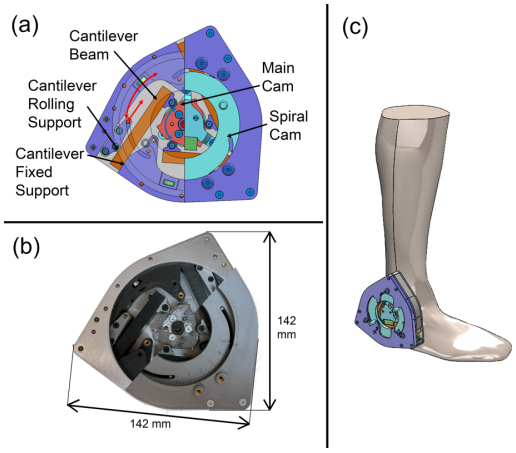

Fig. 1. Internal variable stiffness mechanism section shown, (a) CAD and (b) physical prototpye. (c) Illustration of attachment of the actuator to the human leg. As the main cam (red) rotates, the cantilever beam (orange) are deflected and provide a reaction torque on the cam based on the position of the cantilever rolling supports. The spiral cam (cyan) sets the position of the rolling support.

supports with the assumptions of small deflections and applied loads are orthogonal to the neutral axis of the beam. The linear elastic behavior of beams facilitates them to function as linear spring elements with a displacement corresponding to the beam deflection. Variations in the support type, support, and load locations, bending modulus of elasticity, and cross-sectional properties such as second moment of area are design parameters to consider when defining the stiffness of the cantilever beam element.

Beams are a common mechanism [18] for VSAs in an independent motor setup [2] because the support locations can be changed by applying a force perpendicular to the applied load P. This type of VSAs belong to a family called mechanical impedance adjusters [6] in which the support location can be adjusted by different means of actuation such as lead screws, belt and pulley, cam, etc. [18], [19].

Three potential cantilever beam designs were assessed (Fig. 2) with the objective of optimizing the range of stiffness, while ensuring structural safety factors are maintained. All properties of the beam were kept constant for this trade study except for the support distance, a, which was varied over a consistent range. Additionally, larger deflections were necessary due to improved normalized torque performance of the cam model. Candidate (c) had the largest normalized stiffness range followed by (b) then (a). However, minimal deflections were required to meet safety factors by candidate (c) which degrades its torsional performance and thus (b) was selected.

B. Cam Displaced Cantilever Beam

Cams are mechanical linkages used in many machines where rotary motion is typically converted to linear motion of a follower which is displaced as a function of the cam angle. The cam does work on the follower to raise it to a position of higher potential energy. Polar equations best describe the radius at the point of contact with the follower as a function of the input angle. Under the assumption that the radius of the cam surface is not constant, the slope of the cam will cause the normal contact force to not pass through the center of rotation

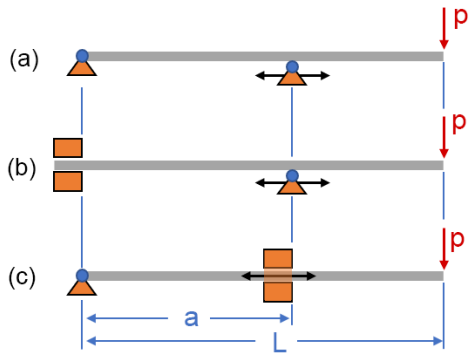

Fig. 2. Candidate cantilever beam structures, pined end with (a) a moving rolling support, (b) fixed end with a moving roller support, (c) and moving fixed support.

and therefore impart a torque on the cam. Carefully selecting the cam trajectory and using the follower to displace the cantilever beam allows the system to function as a torsional spring.

By varying the cam trajectory, this system structure presents the ability to tailor the torsional stiffness properties as a function of the cam angle. By prescribing a stiffness curve for highly cyclic actuation [19], it is possible to alleviate demand on the primary variable stiffness mechanism and reduce wear and actuator extend life.

C. Symmetric Support Positioning Architecture

The actuator is configured such that the cantilever beam and cam are symmetrically patterned around the axis of rotation. By symmetrically arranging the device in this way, the net force on the radial bearings that support the cam is near zero. Additionally, positioning the cantilever beams and rolling supports around the main cam in this manner enables alternative mechanisms to vary the primary variable stiffness mechanism. The path of the rolling supports is such that shifting from a low setting to a high setting result in a reduction in the radius. To continuously position the rolling supports, the system uses a variant of the Archimedean spiral [20] as a cam that modulates the radius as a function of the spiral cam angle. The pressure angle of the spiral cam path with the follower path must be large enough to constrain and drive the follower. The choice of a follower path varies the pressure angle as a function of the angle; thus, the spiral cam path requires a nonlinear trajectory.

III. Design And Fabrication

A. System Design and Considerations

The primary goal of this variable stiffness actuator is to assist users in the task of normal walking. The normalized joint power and ankle angle as a function of gait phase is shown (Fig. 3). The ankle angle increases during the stance phase and the energy is released during toe-off at around 50% gait phase. Then after 50% gait phase, the angle in the plantarflexion direction is large, and the joint power is zero because the joint is unloaded. The principle of this device is to design the VS-SCA with high stiffness during the stance phase, dorsiflexion,

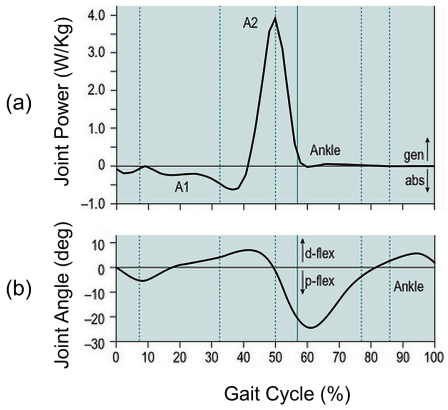

Fig. 3. (a) Joint power largest just before toe-off. (b) The ankle angle dorsiflexes after heal strike (b) [26].

and with low stiffness to minimally impeding plantarflexion during the swing phase.

The radius of the VS-SCA device is vertically constrained such that the actuator doesn't intersect with the ground based on the user-dependent ankle axis height. Thus, VS-SCA has an overall size of 142mm x 142mm x 35mm (Fig. 1). Additionally, weight should be minimized, and the overall stiffness-to-weight ratio should be maximized within manufacturing constraints.

The range of motion is a critical consideration as improper definition could lead to user discomfort or instability during walking [22]. Additionally, the equilibrium position of an elastic mechanism relative to the normal walking equilibrium position is a design variable which can be adjusted for various outcomes [22], [23], [24]. It can be statically biased to enhance energy storage during the stance phase. To ensure higher energy storage in the stance phase with the trade-off of lowering the toe closer to the ground, the local minimum angle, -7°, occurring at ~7% gait cycle is set as the equilibrium bias as shown in (Fig. 3).

B. *Cantilever Beam Design*

Using the Euler-Bernoulli beam theory [21] and applying the elastic boundary conditions (Fig. 4), the elastic curve is broken up in the two parts separated by the rolling support as:

$$v(\mathrm{x}) = \begin{cases} v_1(x) : 0 < x < a \\ v_2(x) : a < x < L \end{cases} \tag{1}$$

$$v_1(x) = \frac{1}{EI}\left(\frac{(P - F_a)x^3}{6} - \frac{(PL - F_a a)x^2}{2} + \theta_s x\right) \tag{2}$$

$$v_2(x) = \frac{1}{EI}\left(\frac{Px^3}{6} - \frac{PLx^2}{2} + \left(\frac{F_a a^2}{2} + \theta_s\right)x - \frac{F_a a^3}{6}\right) \tag{3}$$

where the elastic boundary conditions are defined as:

$$M_b = -k_f \theta_s \tag{4}$$

$$F_a = -k_a y_a \tag{5}$$

Substituting (4) into the moment equilibrium at $x = 0$, then solving for θ_s

$$\theta_s = -\frac{PL + k_a y_a a}{k_f} \tag{6}$$

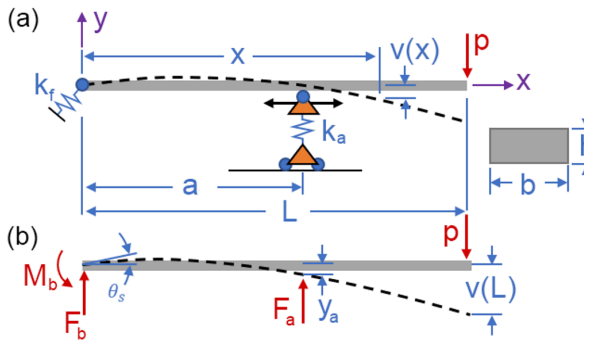

Fig. 4. (a) Semi-fixed-end support with moving flexible roller support cantilever beam model. (b) Free Body Diagram (FBD) with angular and linear displacement compatibilities, θ_s and y_a respectively.

Substituting (5), (6) into (3) where $x = a$, then solving for y_a

$$y_a = -P\left(\frac{3k_f La^2 - k_f a^3 + 6aL}{6k_f EI + 6k_a a^2 + 2k_a k_f a^3}\right) \tag{7}$$

Finally, substituting (6), (7) into (3) where $x = L$, the end deflection is:

$$v_L = \frac{P}{6EIk_f}\left(C_4\left(3k_f k_a a^2 L + 6k_a aL - k_f k_a a^3\right) - 2k_f L^3 - 6L^2\right) \tag{8}$$

$$C_4 = \frac{3k_f La^2 - k_f a^3 + 6aL}{6k_f EI + 6k_a a^2 + 2k_a k_f a^3} \tag{9}$$

The material of the cam was chosen based on analytical evaluation of a number of materials including G10 fiberglass and 301 stainless steel as these or similar materials had been used previously [18], [19]. Trade studies indicated the torsional stiffness performance of the fiberglass was superior because the lower elasticity allowed the cam to increase deflection and therefore increase the moment arm.

The cantilever beam dimensions were determined to maximize length within the envelope, enhancing stiffness range and maximum load capacity, while also reducing the impact of structural stiffness and improving torque output; thickness selection was based on prototype stock sizes, with potential for further optimization in future work, similar to the approach used by Shepherd and Rouse [19] with nonuniform thickness.

The supports used were chosen to best mimic the ideal support conditions, so the fixed support was realized using a pattern of four fasteners to couple it to the base structure. The rolling support simply used a set of rollers in direct contact with the cantilever beam. Lastly, the applied load was realized using an offset roller which engages the main cam.

C. *Cam Design*

The primary considerations of the design of the main cam mechanism are deflection and maximizing the effective moment arm to increase torque output. Polar equations were used to define the follower trajectory (r) for a given input angle of the cam (θ) as:

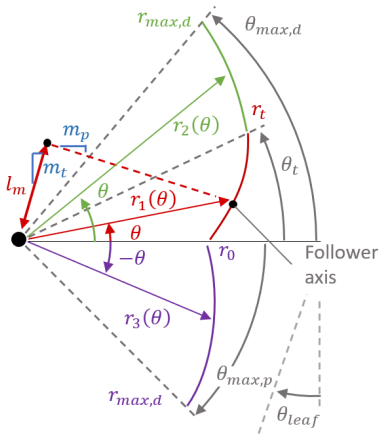

Fig. 5. Main cam follower axis trajectory curve schematic. Cam input angle, θ, results in a displacement of the follower according to the respective polar function. Moment arm, l_m, is perpendicular to the normal contact line.

$$r(\theta) = \begin{cases} r_1(\theta) : 0 < \theta < \theta_t \\ r_2(\theta) : \theta_t < \theta < \theta_{max,d} \\ r_3(\theta) : \theta_{max,p} < \theta < 0 \end{cases} \quad (10)$$

$$r_1(\theta) = \frac{r_t - r_0}{\theta_t}\theta + r_0 \quad (11)$$

$$r_2(\theta) = \frac{r_{max,d} - r_t}{\theta_{max,d} - \theta_t}(\theta - \theta_t) + r_t \quad (12)$$

$$r_3(\theta) = \frac{r_{max,p} - r_0}{\theta_{max,p}}\theta + r_0 \quad (13)$$

The moment arm as a function of θ is determined by first finding the slope at the follower contact point. In Cartesian coordinates, the slope of a curve, i.e., the derivative $\frac{dy}{dx} = \frac{dy}{d\theta}\frac{d\theta}{dx}$, can be determined within the range $0 < \theta < \theta_t$ by finding parametric equations $x(\theta)$ and $y(\theta)$, and then applying them to equation (14). A similar approach is followed for all cam regimes.

$$m_t = \frac{\frac{r_t - r_0}{\theta_t}\sin\theta + \left(\frac{r_t - r_0}{\theta_t}\theta + r_0\right)\cos\theta}{\frac{r_t - r_0}{\theta_t}\cos\theta - \left(\frac{r_t - r_0}{\theta_t}\theta + r_0\right)\sin\theta} \quad (14)$$

$$m_p = -\frac{1}{m_t} \quad (15)$$

The intersection of a line passing through the axis of rotation with slope (m_t) and the perpendicular line with slope (m_p), which passes through the contact point, yields the moment arm (l_m) as:

$$l_m = x_{int}\sqrt{m_t^2 + 1} \quad (16)$$

$$x_{int}(\theta) = \frac{-m_p r_1(\theta)\cos\theta + r_1(\theta)\sin\theta}{m_t - m_p} \quad (17)$$

Normally, spring deflection aligns horizontally, but in this case, the line of action of the cam consistently maintains a relative angle with respect to the horizontal line. However, since the performance of this actuator aims to optimize and increase stiffness in the dorsiflexion direction and minimize in the plantarflexion direction, the cantilevers are rotated such that the line of action is in line with the applied load on the following range, $0 \le \theta \le \theta_t$. This angle is denoted θ_{leaf} in (Fig. 5). This change decreases the complexity of the model as the contact force is equal to the cantilever applied load.

D. Spiral Cam Design

The primary function of the spiral cam is to set the position of all the rolling supports simultaneously. Due to the effective change in radius of the rolling support follower from the low stiffness setting up to the high stiffness setting, a patterned Archimedean spiral [20] is an elegant low-profile mechanism to vary stiffness. However, early testing with a linear spiral indicated the pressure angle of the cam path with respect to the follower was not constant and approached zero as the stiffness increased. Pressure angle is directly related to the controllability and reliability of the rolling support position. Therefore, an alternate spiral cam trajectory was experimentally determined which aims to maintain a constant pressure angle over the full range of motion of the spiral cam angle, θ_s. These coefficients are summarized in TABLE I.

TABLE I. SPIRAL CAM CURVE PARAMETERS

Variable	Value
r_{sm} [1]	0.0393
c_1	0.0060
c_2	-0.4500
c_3	-0.0176
c_4	0.3300
c_5	0.0240
c_6	0.3200

[1]Value set based radius measured from the spiral cam axis to the carrier follower at the maximum stiffness setting.

$$r(\theta) = r_{sm} + c_1(\theta - c_2) + c_3(\theta - c_4)^2 + c_5(\theta - c_6)^3 \quad (18)$$

E. Fabrication

The manufacturing methods to produce this prototype were limited to Fused Deposition Modeling (FDM) additive manufacturing and laser cutting of all the planar steel and aluminum parts. With these constraints, we opted for a stacked architecture with the FDM components having all the non-planar complexity and the planar laser cut parts were integrated where contact loads are applied and to ensure the device doesn't expand under the outward directed loads applied by the rolling supports. Where contact loads are applied, 4130 Chromoly with a 200-300 Brinell Hardness, was used. For the top and bottom plates which resist expansion, 5052 aluminum alloy was used.

IV. VALIDATION OF VS-SCA

A. Analytical Model

The scope of the complete analytical model is to input an angular deflection of the main cam and spiral cam then output a torque of the device. This deflection and torque can then be

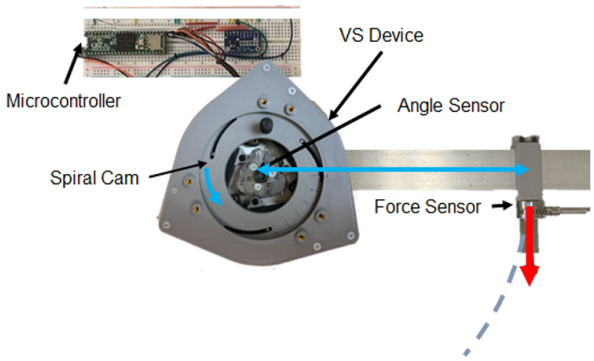

Fig. 6. Experimental setup for stiffness characterization. A load cell is mounted orthogonal to a known moment arm and an encoder measures the cam rotation. A microcontroller collects force and angle data.

used to find an effective torsional stiffness. Given the subsystems (i.e., cantilever beam model, cam, and spiral cam) have been explained in Section III, only the connections between subsystems are reported in this section.

Starting with the spiral cam, the objective is to find the linear displacement of the rolling support which can then be used as an input to the cantilever beam model. A path, symbolizing the rolling support follower's motion, intersects the curve representing the spiral cam's trajectory at a given angle, θ_s. This intersection is determined while considering the angle, θ_{leaf}. There is no closed form solution for the intersection point, so this is computed numerically which then determines the displacement of the rolling support, a, in (8)-(9).

The cam model can then be displaced by an angle, θ, and depending on the value, the radius is adjusted according to (10)-(13). If the cantilever were normal to the cam, $\theta_{leaf} = 0$, the deflection would simply be $r(\theta) - r_0$. However, the relative angle of the cantilever with respect to the cam, θ_{leaf}, reduces the deflection of the cantilever by the $cos(\theta_{leaf})$. Considering the load, the shift angle, θ_{leaf}, is chosen such that the force and line of action are approximately colinear such that, $0 \leq \theta \leq \theta_t$, thus the torque is simply $\tau = Pl_m n$ where n is the number of cantilever beams.

With the above connections of the various subsystems, the output torque, τ, can then be divided by the input main cam angle, θ, which is effectively the torsional stiffness, k_{eq}.

B. Stiffness Characterization Methods

The benchtop experimental setup is shown in (Fig. 6) and is comprised of a load cell (Futek, LCM300, 50lb) rigidly mounted to a torque arm 0.25 m from the axis of rotation. A magnetic angle encoder (AMS, AS5048, 14-bit) measures the rotation of the main cam and torque arm via its diametric magnet affixed to the cam. Both signals are recorded on the microcontroller (Teensy 3.5) for later analysis.

The spiral cam is set in each of the 5 settings (0, 60, 71, 78, 83.2) via a reference scale and viewer printed on the components. The data were collected in the following order (0, 1, 2, 3, 4, 0, 1, ..., 2, 3, 4) testing each setting 5 times. Set screws were tightened on the spiral cam to ensure the setting was maintained under load. The stiffness test consisted of

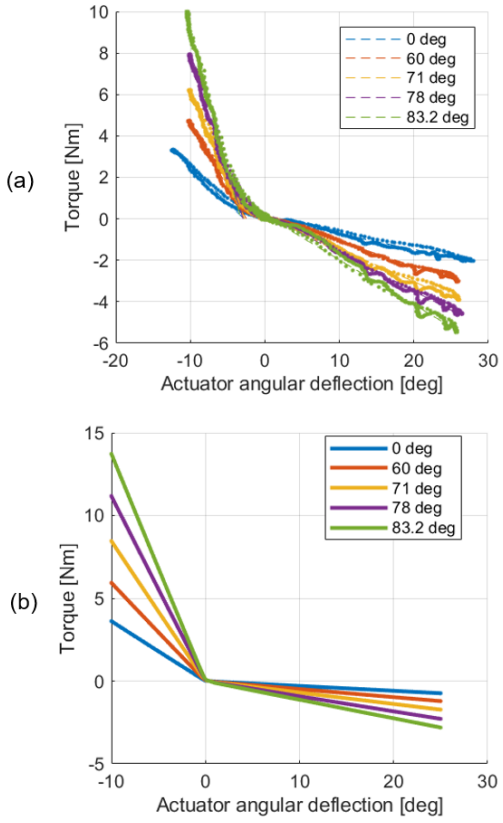

Fig. 7. (a) Actuator torque vs. angular deflection curve for various spiral cam setpoints θ_s, (b) Analytical actuator torque vs. angular deflection curve for various spiral cam setpoints θ_s.

applying a load to deflect the cam to ~10° in dorsiflexion and ~25° in plantarflexion.

Through the process of testing, the support structure stiffnesses k_a and k_f were estimated using a least squared fit of the various configuration data. The fixed support stiffness, k_f, was determined by setting the spiral cam to setting 0 (i.e., $\theta_s = 0°$), which effectively removes the contribution of the rolling support thus is independent from k_a. The value of k_f was then adjusted until the measured stiffness was reached. To find k_a, the spiral cam was set to 4, or $\theta_s = 83.2°$, and the value of k_a was adjusted until the measured stiffness was reached. This version was created by the considering the calculated values of $k_a = 1131.3\ kN/m$ and $k_f = 15.0\ Nm/rad$.

C. Results

The actuator torque vs. angular deflection trajectories for all spiral cam angle samples are reported for both experimental results and analytical model (Fig. 7). The dorsiflexion direction is shown in the negative direction and plantarflexion is shown in the positive direction. Note that the complete range of motion ($-30° \leq \theta \leq 45°$) is not shown and only the expected range covered during normal walking is reported. The experimental result (Fig. 7(a)) trends well with the analytical model (Fig. 7(b)) where the dorsiflexion slope is significantly greater than plantarflexion. The increment in stiffness between tested angles is well predicted.

TABLE II. ACTUATOR STIFFNESS PERFORMANCE, PLANTARFLEXION, DORSIFLEXION

Spiral Cam Angle, θ_s	Actual Plantarflexion Stiffness[2] [Nm/rad]	Analytical Plantarflexion Stiffness[1] [Nm/rad]	Actual Dorsiflexion Stiffness[2] [Nm/rad]	Analytical Dorsiflexion Stiffness[1] [Nm/rad]
0°	4.1 ± 0.6	1.7	19.9 ± 1.1	20.7
60°	7.2 ± 1.0	2.8	36.6 ± 1.7	34.0
71°	9.0 ± 1.2	4.0	50.3 ± 3.0	48.4
78°	10.5 ± 0.7	5.2	63.6 ± 2.0	64.0
83.2°	12.1 ± 0.6	6.4	75.6 ± 1.8	78.6

[1]Analytical model is used along with structural stiffness coefficients k_a and k_f found by measurement with $\theta = 25°$, for plantarflexion, and $\theta = 10°$, for dorsiflexion.

[2]Confidence interval of 95%.

On the dorsiflexion side, there is a gradual increase in stiffness to approximately $-4°$ which is due to a transition designed into the main cam which allows for more gradual application of load to the user. This is the cause for the reduced overall torque output for the same stiffness of the analytical model. When the dorsiflexion stiffness was calculated in the range of $-10°$ to $-4°$, the experimental results are well aligned with the analytical predictions with the percent error from -7% to 4% (Table II). The range of stiffness at various settings varies as follows: At $0°$ spiral cam angle, the lowest setting, the actual stiffness is $19.9\ Nm/rad$ and the max torque is $3.4\ Nm$. The highest setting at $83.2°$ spiral cam angle produces a high stiffness of $75.6\ Nm/rad$ and the max torque is $10.1\ Nm$. Thus, the maximum stiffness achievable by this actuator for dorsiflexion is 3.8 times larger than the minimum stiffness which is appropriate for the application to a wide range of users or walking tasks.

In the plantarflexion direction, the range of stiffness modulation is much smaller than that in the dorsiflexion direction. The maximum stiffness of $12.1\ Nm/rad$ in the plantarflexion direction is significantly lower than the minimum stiffness of $19.9\ Nm/rad$ in the dorsiflexion direction. The maximum resisting torque at $83.2°$ is less than $5\ Nm$, which is low enough no to hinder the natural swing motion [25]. The maximum absolute error between the analytical model and the experimental data is $5.7\ Nm/rad$ and is mainly due to the selection of k_a and k_f parameter to improve model correlation in the dorsiflexion direction.

V. DISCUSSION

The study aims to address the need of assisting human joint power during gait using the proposed VS-SCA. This VSA utilizes joint angles controlled by a spring mechanism, to manage kinetics of motion during normal walking resulting in a passive device. The novel multiple symmetric cams ensure an adjustable architecture and minimal radial load, offering variable stiffness at different cam angles without a large structure. The VSA demonstrates high range of stiffness, from 20 to 75 Nm/rad in dorsiflexion direction, also achieving low range of modulation in plantarflexion direction, with low maximum stiffness of 19.9 Nm/rad, confirming no hindrance to natural motion during walking, ensuring the VSA's ability to assist in gait.

The results observed in the actual testing for dorsiflexion show minimal and acceptable deviation of 5% from the analytical values. However, noticeable errors between the actual and analytical stiffness values are seen in the plantarflexion direction due to the limitations of the Euler-Bernoulli beam theory [21] and the manufacturing imperfections seen on the cam. As per the beam theory, the analytical model doesn't account for axial loads, and the moment arm varies based on the increase in the stiffness. Additionally, considering an error in the manufacturing of the cam, being laser cut, with noticeable undulations on the surface in the plantarflexion direction relative to the dorsiflexion direction, drastic changes in the relative angle of cantilever with respect to the cam path are observed in this regime. This explains the large deviation between the two results in the plantarflexion direction.

The new spiral cam design was created to modulate the support location of each cantilever beam simultaneously. However, to achieve appropriate bearing force to move the support, a nonlinear Archimedean spiral cam path was chosen to maintain a constant pressure angle with most of the variation occurring at the high stiffness regime, $60° \leq \theta_s \leq 83.2°$. The design was optimized to control the sensitivity to the change in angle, θ_s. A future exercise of accurately setting the spiral cam as a closed loop actuator will further improve this design by overcoming minor friction and hysteresis.

Lastly, to enhance the design we can characterize individual components, i.e., the parts like cantilever beam, cam, and the spiral cam. By conducting an extensive characterization of the material for the cantilever beam in a future investigation, the favorable properties, which have a significant effect on the torque and stiffness performance of the actuator, can be elevated. This work will also alleviate some of the inaccuracies of the cantilever beam improving the correlation of the k_a and k_f stiffnesses during characterization testing.

As this is the initial development of this specific VSA, there are opportunities for improvement and further exploration of its applications as discussed above. Integrated testing will involve motor-controlled stiffness adjustments, precision gear train utilization, and position feedback from the spiral cam or carriers, for higher accuracy. Future studies focusing on the development of a controller to manage desired stiffness set points and their timing, will improve the behavior of the mechanism near its equilibrium point, where stiffness adjustments are limited. Structural enhancements, particularly in the carriers, offer potential for optimizing stiffness-to-weight ratios. Furthermore, potential applications may demand automated adjustment of the actuator's equilibrium point for varying slopes [22], [23], and [24].

The principle of this mechanism is optimized for energy storage and release through the main cam's cyclic motion and adaptable global stiffness via the spiral cam. Therefore, human testing will involve its integration into an ankle-foot-orthosis. While this VSA was designed to assist walking of healthy and elderly people, its compact design and novel approaches also have the potential to help patients with ankle impairments or gait disorders. Thus, the VS-SCA has versatile applications in gait assistance, rehabilitation and beyond.

REFERENCES

[1] A. Gefen, "Simulations of foot stability during gait characteristic of ankle dorsiflexor weakness in the elderly," IEEE Transactions on Neural Systems and Rehabilitation Engineering, vol. 9, no. 4, pp. 333 - 337, 2001.

[2] S. Wolf, G. Grioli, O. Eiberger, W. Friedl, M. Grebenstein, H. Höppner and E. Burdet, "Variable Stiffness Actuators: Review on Design and Components," IEEE/ASME Transactions on Mechatronics, vol. 21, no. 5, pp. 2418 - 2430, 2016.

[3] A. M. Sundaram, W. Friedl and M. A. Roa, "Environment-Aware Grasp Strategy Planning in Clutter for a Variable Stiffness Hand," in IEEE/RSJ International Conference on Intelligent Robots and Systems (IROS), Las Vegas, 2020.

[4] Y. Liu, S. Guo, S. Zhang and L. Boulardot, "Modeling and Analysis of a Variable Stiffness Actuator for a Safe Home-based Exoskeleton," in IEEE International Conference on Mechatronics and Automation (ICMA), Changchun, 2018.

[5] Z. Mao, C. Wang, Y. Rui, X. Huang, Z. Zhang, Y. Li and Y. Yang, "Variable Stiffness Mechanism for Single-Joint Lower Limb Wearable Exoskeleton: A Review," in International Conference on Automation, Control and Robots (ICACR), Shanghai, 2022.

[6] R. V. Ham, T. G. Sugar, B. Vanderborght, K. W. Hollander and D. Lefeber, "Compliant Actuator Designs," IEEE Robotics & Automation Magazine, vol. 16, no. 3, pp. 81-94, 2009.

[7] R. Mengacci, M. Garabini, G. Grioli, M. G. Catalano and A. Bicchi, "Overcoming the Torque/Stiffness Range Tradeoff in Antagonistic Variable Stiffness Actuators," IEEE/ASME Transactions on Mechatronics, vol. 26, no. 6, pp. 3186 - 3197, 2021.

[8] F. Petit, W. Friedl, H. Höppner and M. Grebenstein, "Analysis and Synthesis of the Bidirectional Antagonistic Variable Stiffness Mechanism," IEEE/ASME Transactions on Mechatronics, vol. 20, no. 2, pp. 684 - 695, 2015.

[9] Z. Liu, H. Jin, H. Zhang, Y. Liu, Y. Long, X. Liu and J. Zhao, "A Variable Stiffness Actuator Based on Second-order Lever Mechanism and Its Manipulator Integration," in IEEE International Conference on Robotics and Automation (ICRA), Xi'an, 2021.

[10] L. C. Visser, R. Carloni and S. Stramigioli, "Energy-Efficient Variable Stiffness Actuators," IEEE Transactions on Robotics, vol. 27, no. 5, pp. 865 - 875, 2011.

[11] A. Jafari, N. G. Tsagarakis and D. G. Caldwell, "A Novel Intrinsically Energy Efficient Actuator with Adjustable Stiffness (AwAS)," IEEE/ASME Transactions on Mechatronics, vol. 18, no. 1, pp. 355 - 365, 2013.

[12] D. J. Braun, V. Chalvet, T.-H. Chong, S. S. Apte and N. Hogan, "Variable Stiffness Spring Actuators for Low-Energy-Cost Human Augmentation," IEEE Transactions on Robotics, vol. 35, no. 6, pp. 1435 - 1449, 2019.

[13] Y. Xu, K. Guo, J. Li and Y. Li, "A Novel Rotational Actuator with Variable Stiffness Using S-Shaped Springs," IEEE/ASME Transactions on Mechatronics, vol. 26, no. 4, pp. 2249 - 2260, 2021.

[14] J. Liang, Y. Ning, H. Huang, W. Xu, B. Li and Y. Hu, "Design and Modelling of a Modular Variable Stiffness Actuator," in IEEE International Conference on Cyborg and Bionic Systems (CBS), Munich, 2019.

[15] H. J. Bidgoly, M. N. Ahmadabadi and M. R. Zakerzadeh, "Design and modeling of a compact rotational nonlinear spring," in IEEE/RSJ International Conference on Intelligent Robots and Systems (IROS), Daejeon, 2016.

[16] F. Gao, Y. Liu and W.-H. Liao, "A new powered ankle-foot prosthesis with compact parallel spring mechanism," in IEEE International Conference on Robotics and Biomimetics (ROBIO), Qingdao, 2016.

[17] A. Schepelmann, K. A. Geberth and H. Geyer, "Compact nonlinear springs with user defined torque-deflection profiles for series elastic actuators," in IEEE International Conference on Robotics and Automation (ICRA), Hong Kong, 2014.

[18] J. Choi, S. Hong, W. Lee, S. Kang and M. Kim, "A Robot Joint with Variable Stiffness Using Leaf Springs," IEEE Transactions on Robotics, vol. 27, no. 2, pp. 229 - 238, 2011.

[19] M. K. Shepherd and E. J. Rouse, "The VSPA Foot: A Quasi-Passive Ankle-Foot Prosthesis with Continuously Variable Stiffness," IEEE Transactions on Neural Systems and Rehabilitation Engineering, vol. 25, no. 12, pp. 2375 - 2386, 2017.

[20] J. Sun, Z. Guo, Y. Zhang, X. Xiao and J. Tan, "A Novel Design of Serial Variable Stiffness Actuator Based on an Archimedean Spiral Relocation Mechanism," IEEE/ASME Transactions on Mechatronics, vol. 23, no. 5, pp. 2121 - 2131, 2018.

[21] R. C. Hibbeler, "Deflection of Beams and Shafts," in Mechanics of Materials, Hoboken, Pearson, 2017, pp. 577 - 649.

[22] D. Vickers, C. Palk, A. McIntosh and K. Beatty, "Elderly unilateral transtibial amputee gait on an inclined walkway: A biomechanical analysis," Gait Posture, vol. 27, no. 3, pp. 518 - 529, 2008.

[23] E. Nickel, J. Sensinger and A. Hansen, "Passive prosthetic ankle-foot mechanism for automatic adaptation to sloped surfaces," J Rehabil Res Dev., vol. 51, no. 5, pp. 803 - 814, 2014.

[24] M. Alimusaj, L. Fradet, F. Braatz, H. J. Gerner and S. I. Wolf, "Kinematics and kinetics with an adaptive ankle foot system during stair ambulation of transtibial amputees," Gait Posture, vol. 30, no. 3, pp. 356-363, 2009.

[25] A. Moraux, A. Canal, G. Ollivier, I. Ledoux, V. Doppler, C. Payan and J.-Y. Hogrel, "Ankle dorsi- and plantar-flexion torques measured by dynamometry in healthy subjects from 5 to 80 years," BMC Musculoskeletal Disorders, vol. 14, no. 104, 2013.

[26] "Musculoskeletal Key," 26 Dec. 2016. [Online]. Available: https://musculoskeletalkey.com/normal-gait/#bb0250. [Accessed 26 Apr. 2023].